AD-A251 319

TUSKEGEE UNIVERSITY
SCHOOL OF ENGINEERING AND ARCHITECTURE
TUSKEGEE, ALABAMA

DEVELOPMENT OF CAPABILITY FOR CHARACTERIZATION
OF CERAMIC/CERAMIC COMPOSITES
PART - I

(Effects of Reinforcement Geometry on the Mechanical
Properties of $SiCw/Al_2O_3$ Composites and Prediction
of Flexural Properties by Energy Method)

DTIC
ELECTE
JUN 0 1 1992
S
A
D

Shaik Jeelani
Hassan Mahfuz
Anwarul Haque
Sirajus Salekeen

TECHNICAL REPORT

Prepared for

92-14175

92 5 28 132

REPORT DOCUMENTATION PAGE		READ INSTRUCTIONS BEFORE COMPLETING FORM
1. REPORT NUMBER TU-AFSR-2	2. GOVT ACCESSION NO. AEOSR-TR- 92 0451	3. RECIPIENT'S CATALOG NUMBER
4. TITLE (and Subtitle) DEVELOPMENT OF CAPABILITY FOR CHARACTERIZATION OF CERAMIC/CERAMIC COMPOSITES - PART I		5. TYPE OF REPORT & PERIOD COVERED Technical Final Dec.1, 1989– Nov. 30, 1990
		6. PERFORMING ORG. REPORT NUMBER
7. AUTHOR(s) Shaik Jeelani		8. CONTRACT OR GRANT NUMBER(s) F-49620-89-G-0016DEF
9. PERFORMING ORGANIZATION NAME AND ADDRESS Materials Research Laboratory Tuskegee University Tuskegee, AL 36088		10. PROGRAM ELEMENT, PROJECT, TASK AREA & WORK UNIT NUMBERS 61103F, 2312/S5
11. CONTROLLING OFFICE NAME AND ADDRESS AIR FORCE, OFFICE OF SCIENTIFIC RESEARCH BOLLING AIR FORCE BASE, D.C. 20332-6448		12. REPORT DATE January 1991
		13. NUMBER OF PAGES 42
14. MONITORING AGENCY NAME & ADDRESS(If different from Controlling Office) Same as #11		15. SECURITY CLASS. (of this report) Unclassified
		15a. DECLASSIFICATION/DOWNGRADING SCHEDULE

16. DISTRIBUTION STATEMENT (of this Report)

Approved for public release,"
distribution unlimited

17. DISTRIBUTION STATEMENT (of the abstract entered in Block 20, if different from Report)

18. SUPPLEMENTARY NOTES

19. KEY WORDS (Continue on reverse side if necessary and identify by block number)

Composites, Ceramics, Silicon Carbide, Aluminum Oxide, Flexure, Fracture.

20. ABSTRACT (Continue on reverse side if necessary and identify by block number)

This report describes the progress made during the second year of a two-year program funded by the United States Airforce, Office of Scientific Research, to develop experimental and analytical capability to characterize Ceramic/Ceramic composites at room and elevated temperatures.

DD FORM 1473 EDITION OF 1 NOV 65 IS OBSOLETE
1 JAN 73
S/N 0102-LF-014-6601
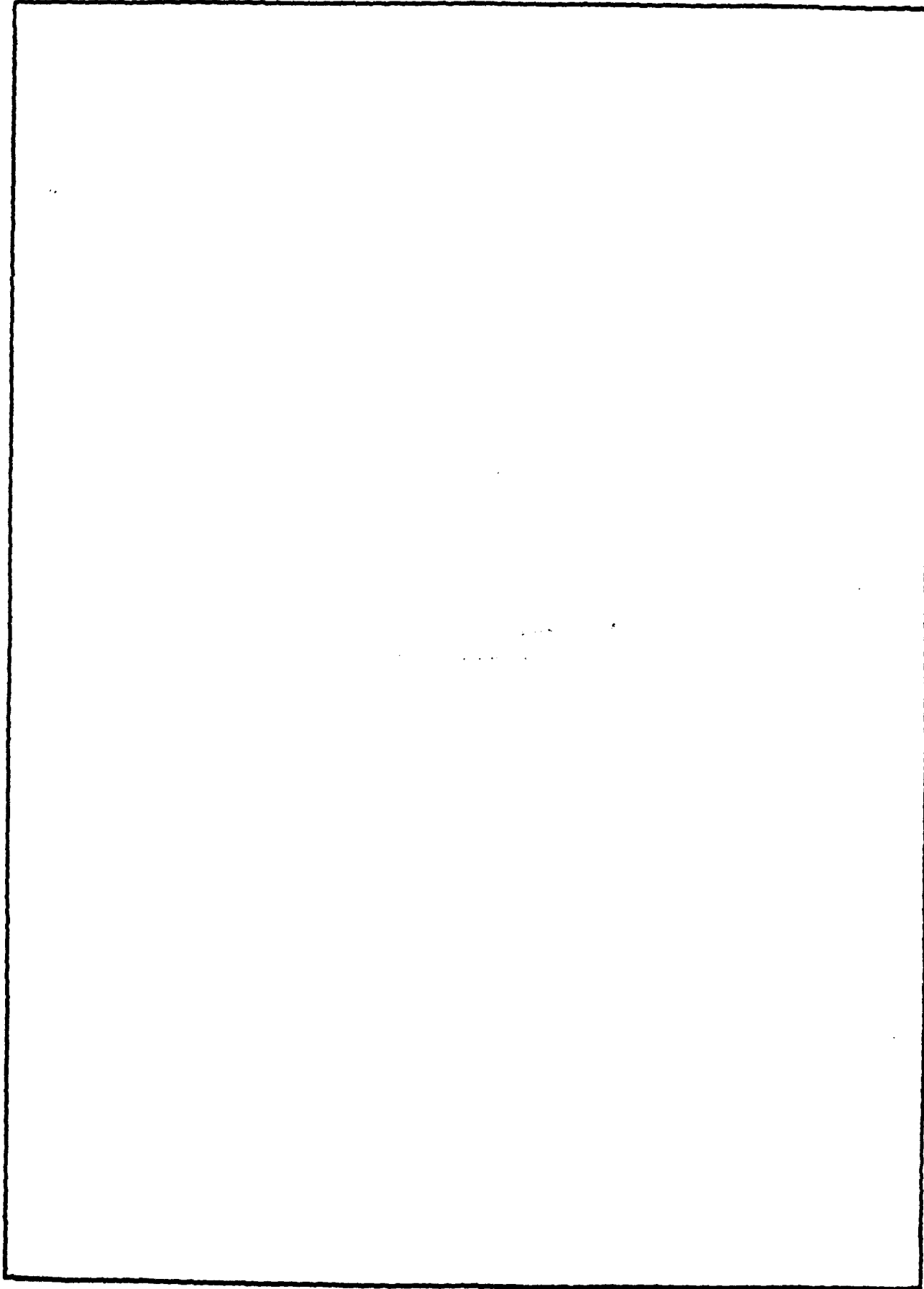
ABSTRACT

The mechanical properties of ceramic composites change due to variations in the size and geometry of the reinforcement. In the present work the effects of SiC whisker (SiC_w) and SiC platelets (SiC_p) have been investigated on the mechanical properties of SiC/Al_2O_3 composites. The flexural properties of both whisker– and platelet–reinforced SiC/Al_2O_3 composites were measured using the four–point bend test. Fracture toughness was determined for both straight and chevron notched specimens. Scanning electron microscopy examination of the fractured surfaces was conducted to perform failure analyses and understand toughening mechanisms.

The results of the investigation indicate that SiC_w/Al_2O_3 composite provides higher flexural strength and fracture toughness compared to SiC_p/Al_2O_3 composite. During the hot pressing, the control of the orientation of the SiC_p is extremely difficult and it appears to form a porous matrix structure which substantially lowers the strength. Moreover, low l/d ratio of SiC_p has a major influence on the fracture toughness. Attempts have been made to predict the flexural properties of the composite by coupling the principle of minimization of potential energy and the rule of mixture. The deflection curve of a composite four–point beam coupon is found from an assumed Fourier series solution satisfying the geometric boundary conditions and using the rule of mixture. Strain compatibility conditions are applied to determine the axial displacement field and hence the flexural strain. Stresses on the matrix and fiber are then estimated under the assumption of isostrain conditions.

1.0 INTRODUCTION

The mechanical properties of monolithic ceramics can be improved significantly by the composite approach. Although the composite properties primarily depend on the materials combination, the shape and micro structural arrangement of the constituents have a significant impact on the mechanical properties of the composites. Whiskers, particles, platelets, fibers, fillers, are most commonly used as reinforcement in structural ceramics. The use of whiskers and platelets in ceramic matrix composites has different implications in terms of orientation, aspect ratio and interface characteristics that control the structural behavior of the composites.

Ceramics, being brittle materials, possess low fracture toughness, restricting their utilization in many structural applications. There has been increased interest in strengthening and toughening of ceramics by the incorporation of particulate or whiskers within the micro structure [1–6]. It has been found that both size and concentration of the dispersed particles influence the fracture toughness [7,8]. Larger dispersed particles contribute to greater toughness than the smaller sizes. The micromechanical residual stresses developed in SiC/Al_2O_3 composites at high temperature appear to be highly dependent on the geometry of the reinforcing inclusion [9]. Crack deflection, fiber breakage, fiber debonding, fiber pullout and wake, etc. are various mechanisms by which whisker or platelets help in toughening the composites [10–12]. It has also been observed that rod–shaped particles are more effective as toughening agents compared to disk or spherical–shaped particles. Considering these various aspects of SiC platelets and SiC whiskers as reinforcements, the present study was undertaken to investigate the influence of both SiC whiskers and platelets in reinforcing the monolithic Al_2O_3. The current research

4

investigated into the improvement of mechanical properties, namely, flexural strength and fracture toughness, due to these reinforcements.

Both flexural strength and fracture toughness in this research were determined using four–point bend test. The governing equation [13–15] to compute the flexural stress in the beam is derived from the Bernoulli–Euler elastic beam theory based on the consideration of equilibrium alone. This does not yield a continuous displacement field that is often required for design purposes. Most importantly, the equation dose not consider anisotropy that exists in the beam materials due to its composite structure. In the current investigation, it is attempted to formulate a method based on the minimization of potential energy, and the rule of mixture to determine the displacement, flexural strain and flexural stress in a four–point beam.

Accesion For		
NTIS CRA&I		☑
DTIC TAB		☐
Unannounced		☐
Justification		
By		
Distribution /		
Availability Codes		
Dist	Avail and / or Special	
A-1		

2.0 EXPERIMENTAL WORK

2.1 Specimen Preparation

The steps involved in processing of Ceramic/Ceramic composites are shown in Fig. 1. The basic raw materials used in the preparation of billets were Al_2O_3 matrix and SiC whisker and SiC platelets. The Al_2O_3 was in the form of powder (EBON A) supplied by Cercom[1]. The SiC whiskers were manufactured by Tokai Carbon[2] with a trade name TWS–100. The SiC platelets were manufactured by American Matrix Inc[3]. The data provided by the manufacturer of Al_2O_3, SiC whiskers and SiC platelets are shown in Tables 1–3.

The SiC whisker or platelets and Al_2O_3 powder were blended by liquid processing to form a slurry. It was then dried under agitation to produce a homogeneous powder. Total reinforcement content was maintained at 30 % by volume. The hot pressing of SiC/Al_2O_3 mixture was carried out at Cercom and Industrial Ceramic Technology[4], in an inert atmosphere of nitrogen using graphite dies. The maximum hot pressing temperature was 1775°C and the maximum pressure applied was 4500 psi. For the fabrication of monolithic alumina billets, the hot pressing was carried at maximum temperature of 1475°C and the maximum pressure applied was 2000 psi. Billets of both monolithic Al_2O_3 and SiC/Al_2O_3 composites were prepared for comparison of the flexural strength and fracture toughness values. All the specimens for flexural strength and fracture toughness were machined and cut as specified in Figs. 2–4. It is well known that whiskers tend to align in the direction perpendicular to the hot pressing axis. Accordingly, attention was given in cutting all the specimens to make certain that the loading axis remained perpendicular to the whisker length as shown in Fig. 5. In the case of platelets such controlled orientation was extremely difficult to achieve through hot pressing.

2.2 Measurement of Flexural Strength

The flexural strength of both whisker– and platelet–reinforced SiC/Al_2O_3 composites and monolithic Al_2O_3 specimens were determined using four–point bend test. Ten specimens of each type were tested to obtain a meaningful Weibull analyses. A ceramic bend fixture with 40 mm outer span and 20 mm inner span was used to conduct the tests. The tests were performed in an Instron load frame with a data acquisition system. The rate of cross head speed was maintained at 0.02 inch/minute.

The flexural strength data of monolithic Al_2O_3 and SiC/Al_2O_3 composite are shown in Table 4. The equation used for determining the flexural strength(four–point loading) is as follows:

$$S_{flex} = 3P(L-a)/2b \tag{1}$$

---

1. Cercom Incorporated, 1960 Watson Way, Vista, CA 92083

2. Tokai Carbon, American Inc., 375 Park Ave., Suit 3802, NY 10152

3. American Matrix Inc., Box 23556, Knoxville, TN 37933

4. Industrial Ceramic Technology, 37 Enterprise Dr., Ann Arbor, MI–48103

Where,

P = Applied load

L = Outer span length

a = Inner span length

b = Width of the specimen

d = Depth of the specimen

2.3 Measurement of Fracture Toughness

The fracture toughness of both whisker and platelet reinforced SiC/Al_2O_3 composites and monolithic Al_2O_3 was measured with two specimen configurations; Straight notched beam [SENB], and Chevron notched beam [CHNB]. The chevron notch configuration as shown in Fig. 6. is characterized by the following parameters: (1) the notch length at the specimen surface, a_1; (2) the notch length to the tip of the chevron a_0; (3) the specimen width, W, and (4) thickness, B. The configuration of the chevron notch used for the experiment is shown in Figure 7. A total number of sixty specimens were tested with approximately ten in each category. In both specimen configurations, the tests were carried out in an Instron load frame with a cross head speed of 0.02 inch/minute. Due to the low load carrying capacity of both the notched specimens, a full scale load of 50 lbs was selected for the test. The fracture toughness data for straight notched and chevron notched specimens are shown in Tables 5 and 6, respectively.

The equation used in calculating the fracture toughness of straight notched specimens is as follows [16]:

$$K_{1c} = \frac{3}{2} \frac{P}{BW^{1/2}} \frac{(S_1 - S_2)}{W} \frac{\Gamma_m \, \alpha^{1/2}}{(1-\alpha)^{3/2}} \qquad (2)$$

8

where,

$$\Gamma_m = 1.9887 - 1.326 \, \alpha - \frac{(3.49 - 0.68 \, \alpha + 1.35 \, \alpha^2) \, \alpha(1-\alpha)}{(1+\alpha)^2} \qquad (3)$$

(3)

$$\alpha = \frac{a}{W}$$

P = Applied load

S_1 = Outer span for loading a 4–point flexural bar specimen

S_2 = Inner span for loading a 4–point flexural bar specimen

B = Width of the specimen

a = Notch length

W = Depth of the specimen

The equation used for determining the fracture toughness of Chevron notched specimens by 4–point bend test is [17]

$$K_{1c} = \frac{P}{BW^{1/2}} Y \qquad (4)$$

where,

$$Y = (2.92 + 4.52\alpha_0 + 16.14\alpha_0^2) \cdot \frac{S_1 - S_2}{W} \cdot \left(\frac{\alpha_1 - \alpha_0}{1 - \alpha_0}\right)^{0.5} \qquad (5)$$

$$\alpha_0 = \frac{a_0}{W} \qquad (6)$$

$$\alpha_1 = \frac{a_1}{W} \qquad (7)$$

P = Applied load

W = Depth of the specimen

B = Width of the specimen

S_1 = Outer span for loading the bar specimen

S_2 = Inner span for loading the 4 point bar specimen

a_0 = Initial notch length (distance from crack mouth to chevron vertex)

a_1 = Distance from crack mouth to intersection of chevron notch & specimen edge

3.0 PREDICTION BY ENERGY APPROACH

The technique of minimizing a particular energy expression and obtaining an approximate solution to the governing differential equation of elasticity is well established and are available in the literatures [18–20]. One of the more important of these techniques is the Rayleigh–Ritz method. In this method the total potential energy, Π is determined by summing up the total strain energy and the total work done, which in turn is estimated from an assumed displacement solution. The assumed displacement solution must satisfy the geometric boundary conditions, and contains unknown constants that are determined by minimizing Π with respect to each of the constants. The rule of mixture is introduced in this formulation with the assumption that both matrix and fiber will contribute to the composite stiffness, E_c in direct proportion to their own stiffness (E_m and E_f) and volume fractions (v_m and v_f). Once the deflection curve is determined, strain compatibility conditions are applied to find the axial displacement field using the symmetry boundary conditions. This yields axial strain which is assumed to be same for both matrix and fiber. Rule of mixture is then applied to compute the stress in the matrix, fiber and in the composite.

3.1 Deflection Solution

A typical four–point beam specimens is shown in Fig. 2. We assume the deflection of the beam as a continuous function of x alone, and approximate it by the following Fourier series. Let u and v be the axial and vertical displacements of the beam, respectively. We assume

$$v(x) = \sum_{n=1}^{\infty} a_n \sin \frac{n\pi x}{L} \tag{8}$$

such that $v(0) = v(L) = 0$ at the two supports of the beam, i.e. at $x = 0$ and $x = L$, respectively. Two simple supports at the two ends can not support any moment and we observe that

$$v''(x) = -\sum_{n=1}^{\infty} a_n \frac{n^2\pi^2}{L^2} \sin \frac{n\pi x}{L} \tag{9}$$

satisfies these two boundary conditions. Therefore four geometric boundary conditions, namely, deflection and moment, at each end of the beam are satisfied.

Let σ_x, σ_y, σ_z, τ_{xy}, τ_{yz}, and τ_{zx} be the state of stress that satisfies the stress equations of equilibrium, and is caused by the application of forces on the surface of the beam. If we denote U to be the total strain energy for the above mentioned stress state, we can write [21]

$$U = \frac{1}{2} \int_v (\sigma_x \epsilon_x + \sigma_y \epsilon_y + \sigma_z \epsilon_z + \tau_{xy}\gamma_{xy} + \tau_{yz}\gamma_{yz} + \tau_{zx}\gamma_{zx})dv \tag{10}$$

However, over the inner span, the beam is under pure bending and we can write $\sigma_x = \sigma$ and $\sigma_y = \sigma_z = \tau_{xy} = \tau_{yz} = \tau_{zx} = 0$. Here σ denotes the bending or flexural stress on the beam due to the applied load. Therefore,

$$U = \frac{1}{2} \int_v \frac{\sigma^2}{E} dv \tag{11}$$

Under the pure bending $\sigma = \frac{My}{I}$ where M and I are respectively the applied moment and

the second moment of the cross–sectional area. The substitution reduces equation (11) to

$$U = \frac{1}{2} \int_0^L \frac{M^2}{EI} dx \qquad (12)$$

It is to be noted here that $\sigma = \frac{My}{I}$ is based on the assumption of homogeneous material and the isotropic Hooke's law. Therefore, eqn. (12) will be modified later by the rule of mixture. In terms of displacement $v(x)$, we can write equation (12) as

$$U = \frac{1}{2} \int_0^L EI \left(\frac{d^2v}{dx^2}\right)^2 dx \qquad (13)$$

where we have substituted $M = EI\dfrac{d^2v}{dx^2}$.

We know that E is not a constant over the volume and herein we introduce the rule of mixture to account for the multi phase materials of the beam specimen. Since the cross–sectional area of the specimen is constant along x, the distribution of E over x is taken from the simple rule of mixture such that

$$E_c = E_m v_m + E_f v_f \qquad (14)$$

Where E_m, E_f, v_m, and v_f's are respectively the elastic modulii and volume fractions of the matrix and the fiber. Here we have assumed that $v_m + v_f = 1$, and both matrix and fiber contribute to the composite stiffness in direct proportion to their respective stiffnesses and volume fractions. Equation (13) therefore, takes the form

$$U = \frac{E_m v_m I}{2} \int_0^L EI \left(\frac{d^2v}{dx^2}\right)^2 dx + \frac{E_f v_f I}{2} \int_0^L EI \left(\frac{d^2v}{dx^2}\right)^2 dx \qquad (15)$$

12

We now proceed to determine the work done, W, on the beam by the applied loads. We can write

$$W = \frac{P}{2}(v)_{x=\frac{L}{4}} + \frac{P}{2} \cdot (v)_{x=\frac{3L}{4}} \tag{16}$$

$$= \frac{P}{2} \left[\sum_{n=1}^{\infty} a_n \sin\frac{n\pi}{4} + \sum_{n=1}^{\infty} a_n \sin\frac{3n\pi}{4} \right] \tag{17}$$

We know from symmetric loading that $(v)_{x=\frac{L}{4}} = (v)_{x=\frac{3L}{4}}$. To conform to this condition, we restrict the values of n = 1, 3, 9, 11....etc. in the infinite series such that

$$W = P \sum_{n=1,3,9,11}^{\infty} a_n \sin\frac{n\pi}{4} \tag{18}$$

The total potential energy, Π can therefore, be written as

$$\Pi = U - W = \frac{E_m v_m I}{2} \int_0^L EI \left(\frac{d^2 v}{dx^2}\right)^2 dx + \frac{E_f v_f I}{2} \int_0^L EI \left(\frac{d^2 v}{dx^2}\right)^2 dx - P \sum_{n=1,3,9,11}^{\infty} a_n \sin\frac{n\pi}{4}$$

$$= \frac{I(E_m v_m + E_f v_f)}{2} \int_0^L \left[\sum_{n=1,3,9,11}^{\infty} a_n \left(\frac{n\pi}{L}\right)^2 \sin\frac{n\pi x}{L} \right]^2 dx - P \sum_{n=1,3,9,11}^{\infty} a_n \sin\frac{n\pi}{4} \tag{19}$$

Squaring the series and observing that

$$\int_0^L \sin\frac{m\pi x}{L} \sin\frac{n\pi x}{L} dx = 0, \text{ for } m \neq n$$

$$\text{and } \int_0^L \sin\frac{m\pi x}{L} \sin\frac{n\pi x}{L} dx = L/2, \text{ for } m = n,$$

we get

$$\Pi = \frac{\pi^4 I(E_m v_m + E_f v_f)}{4L^3} \sum_{n=1,3,9,11}^{\infty} a_n^2 \, n^4 - P \sum_{n=1,3,9,11}^{\infty} a_n \mathrm{Sin} \frac{n\pi}{4} \tag{20}$$

Now we apply the minimizing condition

$$\frac{\partial \Pi}{\partial a_m} = 0 \tag{21}$$

where all coefficients except a_m are taken as constant during the partial differentiation. Differentiating equations (20) according to equation (21) we find that

$$\frac{\pi^4 m^4 I(E_m V_m + E_f V_f)}{2L^3} \cdot a_m = P \, \mathrm{Sin} \, \frac{m\pi}{4}$$

$$\text{i.e,} \quad a_m = \frac{\sqrt{2} \; PL^3}{\pi^4 m^4 I(E_m v_m + E_f v_f)} \tag{22}$$

for $m = 1, 3, 9, 11$ etc.

Therefore, the deflection of the composite beam can be found from equation (8) as

$$v(x) = \frac{\sqrt{2} \; PL^3}{\pi^4 I(E_m v_m + E_f v_f)} \sum_{n=1,3,9,11}^{\infty} \frac{1}{n^4} \mathrm{Sin} \frac{n\pi x}{L} \tag{23}$$

We will use this expression to compute the maximum deflection in the beam which will be compared with the experimentally found values.

14

3.2 Strain and Stress Solution

We have observed before that the existing stress in the beam is only $\sigma_x = \sigma$ with σ_y, σ_z, τ_{xy}, τ_{yz}, and τ_{zx} being zero. Under this condition, we can write the strain compatibility condition as

$$\frac{\partial v}{\partial x} + \frac{\partial u}{\partial y} = 0 \tag{24}$$

From eqn. (24), with the help of eqn.(23), we can write

$$\frac{\partial u}{\partial y} = -\frac{\sqrt{2}\ PL^2}{\pi^3 I(E_m v_m + E_f v_f)} \sum_{n=1,\,3\,,\,9,\,11}^{\infty} \frac{1}{n^3} Cos\frac{n\pi x}{L} \tag{25}$$

Integrating equation (25) with respect to y

$$u = -\frac{\sqrt{2}\ PL^2 y}{\pi^3 I(E_m v_m + E_f v_f)} \sum_{n=1,\,3\,,\,9,\,11}^{\infty} \frac{1}{n^3} Cos\frac{n\pi x}{L} + f(x) \tag{26}$$

To find f(x), we apply the symmetry boundary condition, that at $x = L/2$, $u = 0$ for all values of y. This gives, $f(x) = 0$, therefore, we write

$$u = -\frac{\sqrt{2}\ PL^2 y}{\pi^3 I(E_m v_m + E_f v_f)} \sum_{n=1,\,3\,,\,9,\,11}^{\infty} \frac{1}{n^3} Cos\frac{n\pi x}{L} \tag{27}$$

This is the general expression for u and we observe that it is a function of both x and y. From equation (27) we find the flexural strain, ϵ_x as

$$\epsilon_x = \frac{\partial u}{\partial x} = \frac{\sqrt{2}\ PLy}{\pi^2 I(E_m v_m + E_f v_f)} \sum_{n=1,3,9,11}^{\infty} \frac{1}{n^2} \mathrm{Sin} \frac{n\pi x}{L} \tag{28}$$

We will compute maximum strain in the composite beam according to equation (28) and compare with the experimental value. Assuming isostrain both in the matrix and fiber in the axial direction, we can write

$$\sigma_f = E_f \epsilon_x \text{ and } \sigma_m = E_m \epsilon_x \tag{29}$$

Where σ_m and σ_f are the stresses in the matrix and fiber. Using the rule of mixture we now find the flexural stress in the composite, σ_{comp} [22,23], as

$$\sigma_{comp} = \sigma_f V_f + \sigma_m (1 - V_f) \tag{30}$$

4.0 RESULTS AND DISCUSSION

4.1 Flexure and Fracture Tests

Prior to discussing the results of this study, it is appropriate to discuss some of the limitations of bend tests in measuring the flexural strength and fracture toughness of ceramic matrix composites. The flexural test is commonly employed in strength characterization of ceramic matrix composites due to the problems of gripping and aligning the specimen during the tensile test. The complexity in performing high temperature test with tensile fixture and cost of tensile specimens are major concerns in characterizing ceramic matrix composites. But the common practice of performing bend test appears to give higher strength than the data obtained from a standard tensile coupon for both polymer and ceramic matrix composites [24,25]. Flaws existing in a specimen are subjected to a uniform maximum stress field during tensile loading. However, during flexure, the stress field is almost linearly varying from the neutral axis of the beam cross section. This variation in the stress field reduces the possibility of occurrence of flaws within the maximum stress field, and hence gives higher strength. Again in bend tests, the three–point loading produces higher strength as compared to four–point loading. This is because the smaller volume under maximum stress gives higher local strength. This difference in strength suggests the importance of finding the ratios for characteristic flexural strength to tensile strength using Weibull statistical strength theory for brittle materials [26]. Since Weibull statistics contain a volume term, it can predict the effect of volume on the strength parameter. The four–point loading is often preferred to three–point loading because the center section is under pure bending.

The fracture toughness K_{1c} measured from the existence of critical stress intensity factor K_{1c} is implied to linear elastic fracture mechanics. Ceramic materials behave in a linear elastic manner at least at low temperature, which reasonably justifies the measurement of fracture toughness through K_{1c} value. The four—point bend method with both straight and chevron notched specimens appear to be promising candidates for standard K_{1c} measurement techniques. Despite such presumption, the results show discrepancy in measured values due to the influence of specimen dimensions, loading rates, and loading fixtures which urge a standard test technique to obtain a true K_{1c} value for ceramic materials.

Data for flexural strength of Al_2O_3, SiC_w/Al_2O_3 and SiC_p/Al_2O_3 were analyzed by Weibull distribution curves shown in Fig. 8, to establish the probability of failure occurrence. It is evident from Fig. 8 that the Weibull characteristic life of single phase monolithic Al_2O_3 has been increased almost one and half times due to the incorporation of SiC whiskers, whereas in the case of SiC platelets the strength of the composite has been decreased. Most of the flexural strength data in Figure 8 show linearity and well distributed fit in weibull plot except few in the case of Al_2O_3. The bad fit represent the material behavior or the quality of the data. The asterisk marked data in Al_2O_3 shows a material defect due to a significant lower flexural strength. The value of the shape factor parameter of the monolithic Al_2O_3 would be higher if the asterisk marked data were omitted from the plot. A significant higher value of the shape factor parameter denotes less scatter in data of flexural strength in SiC_w/Al_2O_3.

The difficulty in hot—pressing technique regarding the orientation of the platelets is easily detected from the SEM examinations in Figs. 9–11 . To obtain optimum strength properties in platelet—reinforced composites, flatness and freedom from surface and edge cracks are essential, but a high degree of parallelism in platelet distribution is more

important than the uniformity of the particles themselves. The lack of such parallelism in platelets distribution is revealed in the SEM examination.

Also, whenever a multi phase material is processed at elevated temperatures, the differences in the thermal expansion coefficients and elastic modulii of the phases result in residual stresses upon cooling to room temperature. These residual thermo–mechanical stresses have always been of interest from both the strengthening and the weakening perspective. The geometry of the inclusion, expressed as aspect ratio, (length/diameter or l/d) directly affects the magnitude of this internal stresses [9]. The l/d ratio is a highly significant factor which can either amplify or reduce the thermal and elastic effects on the internal stresses. When the l/d ratio increases, the stress inside the inclusion parallel to the l axis significantly increases, and the tangential stresses parallel to the l axis at the interface of the inclusion decreases. As a result, an inclusion with a whisker shape will carry more unidirectional load than one with a spherical shape. The results of the present study show that composites reinforced with platelets have very low flexural strength and the low l/d ratio of platelets is a significant factor in causing higher residual micromechanical stresses. However experimental investigation of such residual stresses is necessary before drawing any conclusion. The porosity due to incomplete densification is also of critical concern in platelet composites. These defects may be due to improper platelet/powder blending or because of harvesting of SiC platelets prior to the mixing with Al_2O_3. Possible refinements including good dispersion technique in order to avoid agglomeration of platelets in Al_2O_3 matrix and improved harvesting/sizing procedure for platelets are therefore, suggested.

Figures 12 and 13 show the Weibull distribution of fracture toughness of monolithic Al_2O_3, SiC_w/Al_2O_3 and SiC_p/Al_2O_3 composites obtained using four–point bend test for both straight– and chevron notched specimens. A comparison study of the Weibull characteristic values and the average value for both flexural strength and fracture toughness are presented

in Table 7. It is observed that the K_{1c} of Al_2O_3 is increased with the incorporation of SiC whiskers and has a maximum value of 5.09 MPa$\sqrt{m}$ for straight notched specimens and 7.69 for chevron notched specimens. The observed increase in the K_{1c} of Al_2O_3 as a result of SiC whisker addition is due to the changes in the micro structure. It is apparent that the average values are always lower as compared to Weibull characteristic values. It is also evident that the chevron notched specimens show higher K_{1c} values than those of the straight notched specimens for both SiC_w and SiC_p composites. The addition of whiskers to monolithic Al_2O_3 results in crack deflection, whisker pullout, and possibly crack bridging as are evident from the SEM micro graphs (Figure 9) of the fractured surface of the SiC_w/Al_2O_3 specimen. Whisker pullout is detected in both the fractured surfaces. Holes are observed where whiskers dislodged prior to fracture, and in some cases whiskers are observed to be protruding above the fractured surface.

The state of stress at the matrix/whisker interface plays an important role in the toughening mechanisms. Due to the thermal coefficient expansion mismatch of Al_2O_3 and SiC_w, large compressive stresses are developed in the SiC whiskers and tensile stresses are developed in the Al_2O_3 matrix. Since the whiskers are in compression and the matrix is in tension at the interface, the main propagating crack is attracted to the tensile region and is deflected along the interface.

It is clear from Fig. 12 and 13 that the fracture toughness values of the SiC_p/Al_2O_3 composite are significantly lower than that of the monolithic Al_2O_3. The reasons which are described for the discrepancy of flexural strengths are also applicable to the fracture toughness. The SEM micro graphs of platelet composites (Fig. 10 & 11) show less evidence of any commonly implied toughening mechanisms that are observed in whisker composites. Analytical investigations have shown that the degree of toughening depends on the shape

20

and therefore on the surface area of the dispersoid [27]. Both analytical and experimental investigations of the failure mechanisms with different sizes of platelets are necessary for a complete understanding of the effects of such reinforcements.

4.2 Energy Approach:

Values of Maximum deflection, flexural strain and flexural stress obtained from the four–point bend test as shown in the previous section at room temperature, have been considered in the energy approach as a basis of a comparison. Values for both monolithic SiC and SiC_w/Al_2O_3 were compared. Using eqn. (13) for monolithic material, and performing the similar derivations we can easily formulate

$$v(x) = \frac{\sqrt{2}PL^3}{\pi^4 E_m I} \sum_{n=1,3,9,11}^{\infty} \frac{1}{n^4} Sin\frac{n\pi x}{L} \tag{31}$$

$$\text{and} \quad \epsilon_x = \frac{\sqrt{2}PLy}{\pi^2 E_m I} \sum_{n=1,3,9,11}^{\infty} \frac{1}{n^2} Sin\frac{n\pi x}{L}$$

where E_m is the elastic modulus of monolithic SiC. From eqn. (23) we observe that the maximum deflection takes place at $x = L/2$. The series contains $1/n^4$ term which is highly convergent and, therefore, taking only two terms, i.e., with $n = 1$ and 3

$$v_{max} = \frac{\sqrt{2}\ PL^3}{\pi^4 I(E_m v_m + E_f v_f)}[1 - \frac{1}{81}] \tag{32}$$

According to eqn. (28), we can compute maximum strain at $x = L/2$ and at $y = d/2$, where d is the depth of the specimen. Eqn. (28), with two terms in the series, reduces to

$$(\epsilon_x)_{max} = \frac{\sqrt{2}\ PLd}{2\pi^2 I(E_m v_m + E_f v_f)}[1 - \frac{1}{9}] \tag{33}$$

Now taking this maximum strain under consideration, we can determine the flexural stress using eqns.(29) and (30). Computations have been carried out for both monolithic SiC and SiC_w/Al_2O_3 using the following properties:

$E_m = 271.28 \times 10^9\ N/m^2, \quad E_f = 450.0 \times 10^9\ N/m^2,$

$v_m = 0.7, \qquad v_f = 0.3,$

$I = bd^3/12 = 16 \times 10^{-12}\ m^4,$

$L = 0.04\ m, \qquad d = 0.004\ m.$

The comparison with the experimentally determined values are shown in Table–8 and Table–9.

5. CONCLUSIONS

From the results of the investigation the following conclusions can be drawn.

1. The flexural strength and fracture toughness of monolithic Al_2O_3 increase due to incorporation of SiC whiskers. In the case of platelets both strength and toughness of the composites appear to decrease in comparison to monolithic Al_2O_3.

2. It appears that chevron—notched specimens provide higher K_{1c} values than those of the straight notched specimens for both SiC_w and SiC_p composites.

3. Scanning electron microscopy examination reveals that there is lack of parallelism in platelet orientation which necessitates the development of a technique to control the platelet orientation in processing.

4. A formulation based on Rayleigh—Ritz method is presented to compute the deflection of a composite four—point beam specimen that has been used in the current investigation for mechanical characterization. Axial displacement and strain equations are derived from the strain compatibility condition, and stress equations are established on the basis of the rule of mixture and the assumption of isostrain condition. Good correlation between the experimental and predicted values are observed.

6.0 ACKNOWLEDGEMENTS

24

7.0 REFERENCES

1. M. G. Jenkins, A.S. Kobayashi, K.W. White and R.C. Bradt, "Crack Initiation and Arrest in a SiC whisker/Al_2O_3 Matrix Composite, "J. Am. Ceram. Soc., 70[6] 362-05 (1987).

2. G. C. Wei and P.F. Becher, "Development of SiC whisker Reinforced Ceramics," Am. Ceram. Soc. Bull., 65[2] 298-304 (1985).

3. T.N. Tiegs and P.F. Becher, "Whisker-Reinforced Ceramic Composites," Am. Ceram. Soc. Bull.,64 [2] 298-304 (1985).

4. J. Homeny, W.L. Vaughn and M.K. Ferber, "Processing and Mechanical Properties of SiC-Whisker-Al_2O_3-Matrix Composites," Amer. Ceram. Soc. Bull. 66[2]   pp.333-38(1987)

5. L. J. Neergaard and J. Homeny, "Mechanical Properties of Beta-Silicon Nitride Whisker/Silicon Nitride Matrix Composites," Technical Report UIUC-NCCMR-89-0008,Department of Material Science and Engineering, University of Illinois,Urbana-Champaign

6. N. Claussen, "Fracture Toughness of Al_2O_3 with an Unstabilized ZrO_2 Dispersed Phase, " J. Am. Cer. Soc., 59[1-2] 49-51 (1976).

7. S.T. Bulijan and V.K. Sarin, "Silicon Nitride-Based Composites," Composites, 18 [2] 99-106 (1987).

8. S.T. Bulijan, J.G. Baldani, and M.L. Huckabee,"Si_3N_4/SiC Composites," Am. Ceram. Soc. Bull., 66 [2] 347-52 (1987).

9. L. Zhuang and R. C. Bradt., " Micromechanical Stresses in SiC-Reinforced Al_2O_3 Composites," J. Am. Ceram. Soc., 72 [1] 70-77 (1989).

10. P. F. Becher, C. Hsueh, P. Angelin, and T. N. Tigers," Toughening Behavior in Whisker-Reinforced Ceramic Matrix Composite," J. Am. Ceram. Soc., 71[12] 1056-61   (1988).

11. J.P. Singh, S. Smith and R. O. Scattergood," Observation on the Toughening of Al_2O_3-SiC Composites", Materials and Components Technology Division, Argonne National Laboratory, Argonne, Illinois 60439.

12. D. B. Marshall and J. E. Ritter, "Reliability of Advanced Structural Ceramics and Ceramic Matrix Composites - A Review", Ceramic Bulletin, 66, [2], 309-317, 1987.

13. Whitney, J. M., Daniel, I. M. and Pipes, B., **Experimental Mechanics of Fiber Reinforced Composite Materials**, Society for Experimental Stress Analysis, Monograph No. 4.

14. Instron Series IX **Automated Materials Testing System Reference Manual**, M–12–2–152 (a), pp. b–1 to b–6.

15. Zweben, C., Smith W. S. and Wardle, M. W., "Test Methods for Fiber Tensile Strength, Composite Flexure Modulus, and Properties of Fabric–Reinforced Laminates," Composite Materials: Testing and Design (Fifth Conference), ASTM STP 674, 1979, pp. 228–262.

16. Munz, D., Busbey, R. T. and Shannon, J. L., "Fracture Toughness Determination of Alumina Using Four–Point Bend Specimens With Straight–Through and Chevron Notches," Journal of the American Ceram'c Society, Vol. 63, No. 5–6 (1980).

17. Munz, D. J., Shannon, J. L. and Busbey, R. T., "Fracture Toughness Calculation from Maximum Load in Four–Point Bend Tests of Chevron Notch Specimens," International Journal of Fracture, 16R, 137–141 (1980).

18. Chou, P. and Pagano, N., **Elasticity**, D. Van Nostrand Company, Inc., Princeton, New Jersey, 1967.

19. Segerlind, L., **Applied Finite Element Analysis**, 2nd. Edition, John Wiley and Sons, New York, 1984.

20. Budynas, R., Advanced Strength and Applied Stress Analysis, McGraw–Hill Book Company, New York, 1975.

21. Jones, R. M., **Mechanics of Composite Materials**, Hemisphere Publishing Corporation, New York, 1975.

22. Yong, B. K. and Kim, C. H., "The Effect of Whisker Length on the Mechanical Properties of Alumina–SiC Whisker Composites," Journal of Material Science, 24 (1989), 1589–1593.

23. Fukuda, H. and Chow, W.., "A Probabilistic Theory of the Strength of Short–Fiber Composites With Variable Fiber Length and Orientation," Journal of Materials Science 17 (1982), 1003–1011.

24. J. M. Whitney, I. M. Daniel, and R. B. Pipes,"Experimental Mechanics of Fiber Reinforced Composite Materials," pp. 169–171, ed. 1982, Society for Experimental Stress Analysis.

25. P. J. Lamicq, G. A. Bernhart, M. M. Dauchier, and J. G. Mace, " SiC/SiC Composite Ceramics," Am. Ceram. Soc. Bull., 65[2], 336–38(1986).

26. W. Weibull, " A Statistical Theory of the Strength of Materials," Ing. Vetenskaps Akad, Handl., No. 151, 5–45(1939).

27. P. D. Shalek, J. J. Petrovic, G. F. Hurley, and F. D. Gac, " Hot–Pressed SiC whisker/Si_3N_4 Matrix Composites, " Am. Ceram. Soc. Bull., 65[2] 351–56 (1986).

SiC/Al2O3 Processing

```
┌──────────────┐        ┌──────────────┐
│     SIC      │        │    Al2O3     │
└──────┬───────┘        └──────┬───────┘
       │                       │
       └───────────┬───────────┘
                   │
          ┌────────┴────────┐
          │    Blending     │
          └────────┬────────┘
                   │
          ┌────────┴────────┐
          │     Drying      │
          └────────┬────────┘
                   │
          ┌────────┴────────┐
          │  Hot  Pressing  │
          └────────┬────────┘
                   │
          ┌────────┴────────┐
          │   Machining &   │
          │Specimen Preparation│
          └─────────────────┘
```
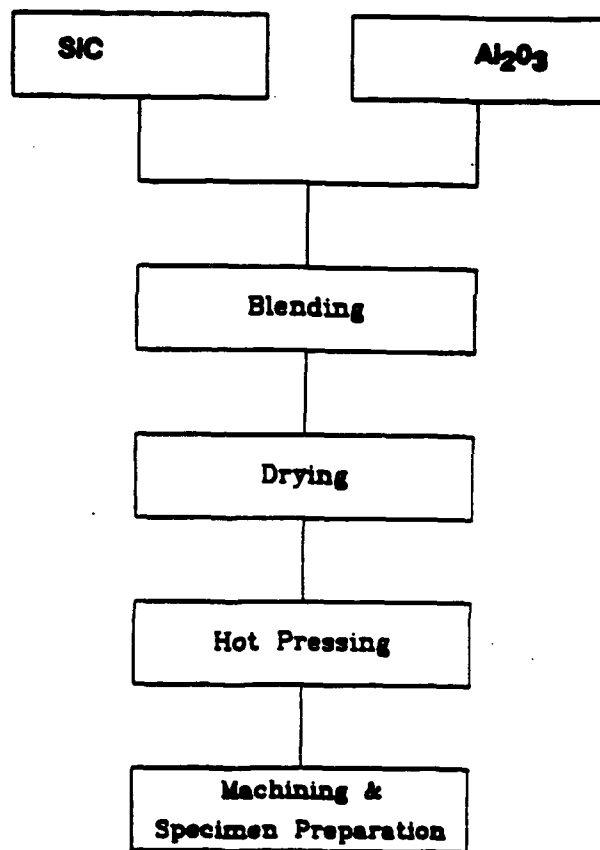
Figure 1 Processing of SiC/Al$_2$O$_3$
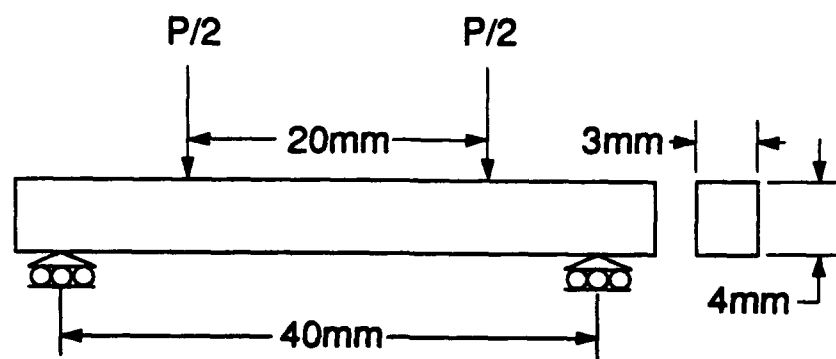
Figure 2 Flexural Test Specimen
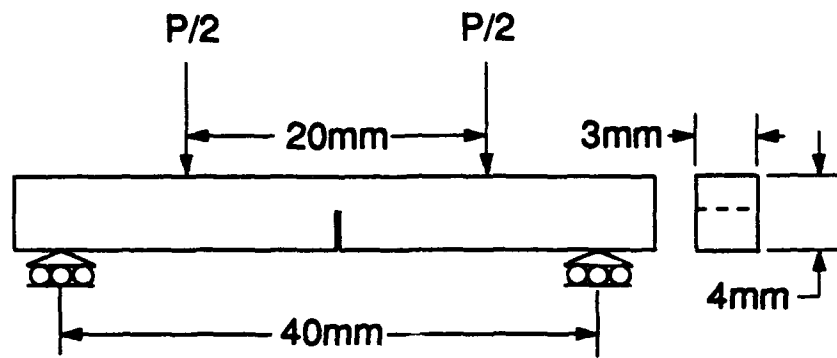
Figure 3   Straight Notched Specimen
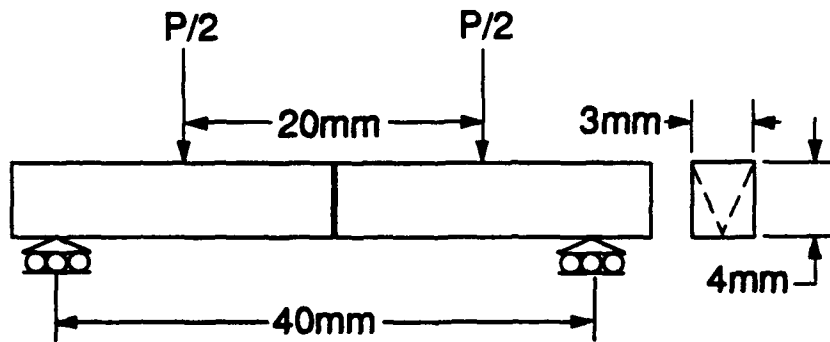
Figure   4   Chevron Notched Specimen

27

HOT PRESSING DIRECTION

3.0 mm

75 mm

14.29 mm

4.0 mm

50 mm

102 mm
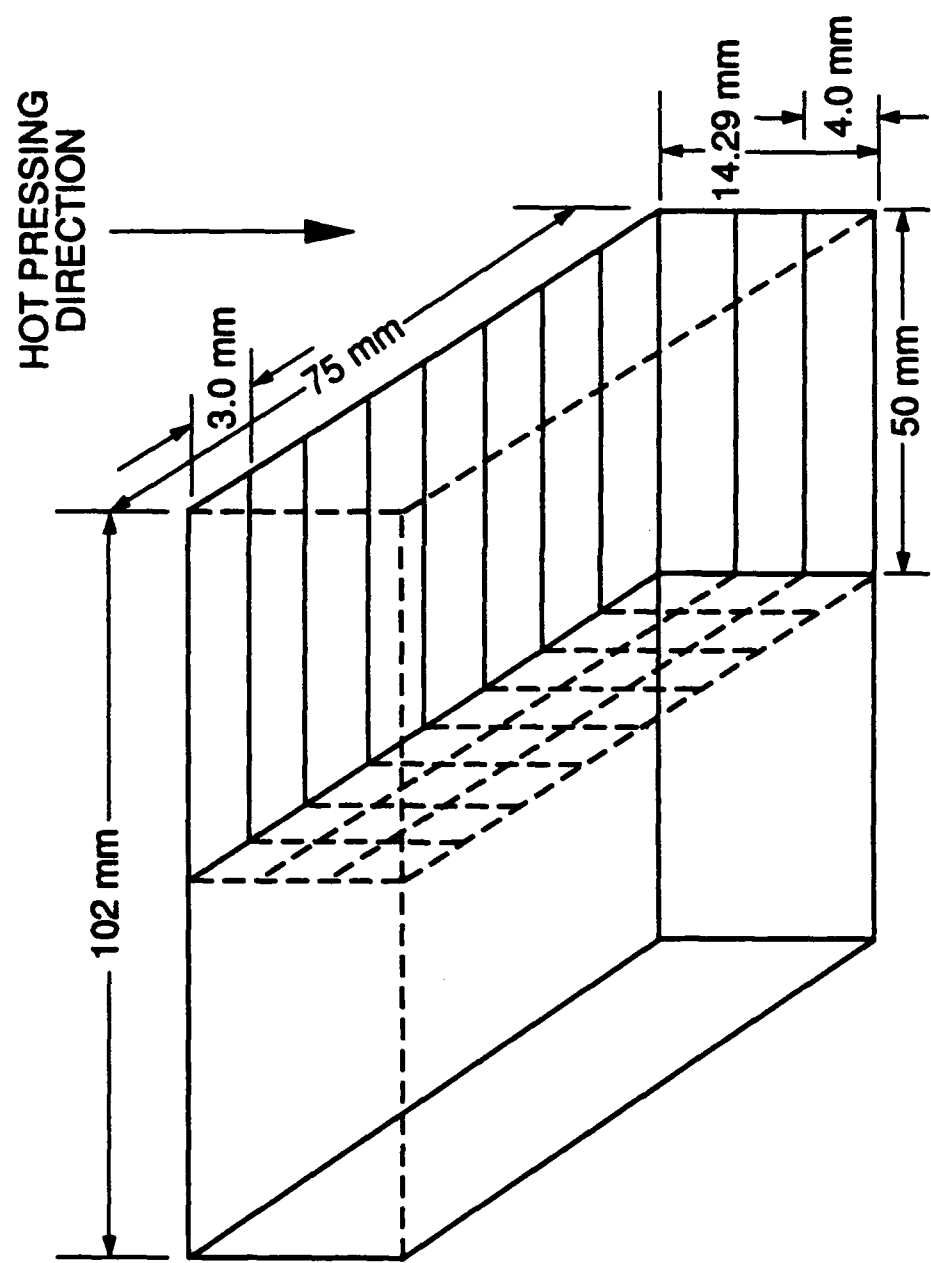
Figure 5 Specimen Orientation in Hot Billet
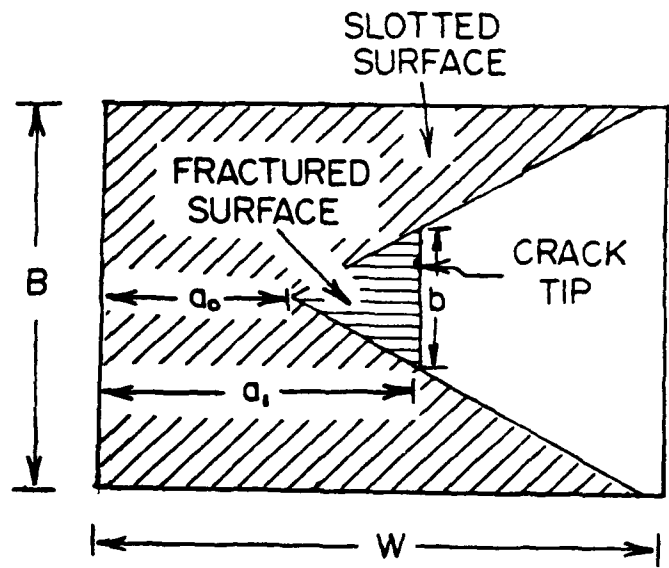
Figure 6 Plan view with of the General Chevron Notched
Fracture Toughness sample with nomenclature
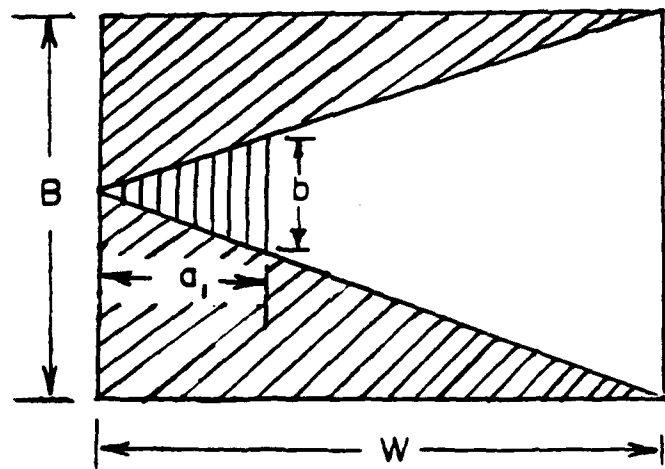
Figure 7 Plan view of the Chevron Notched specimen
used for our experiment.

29
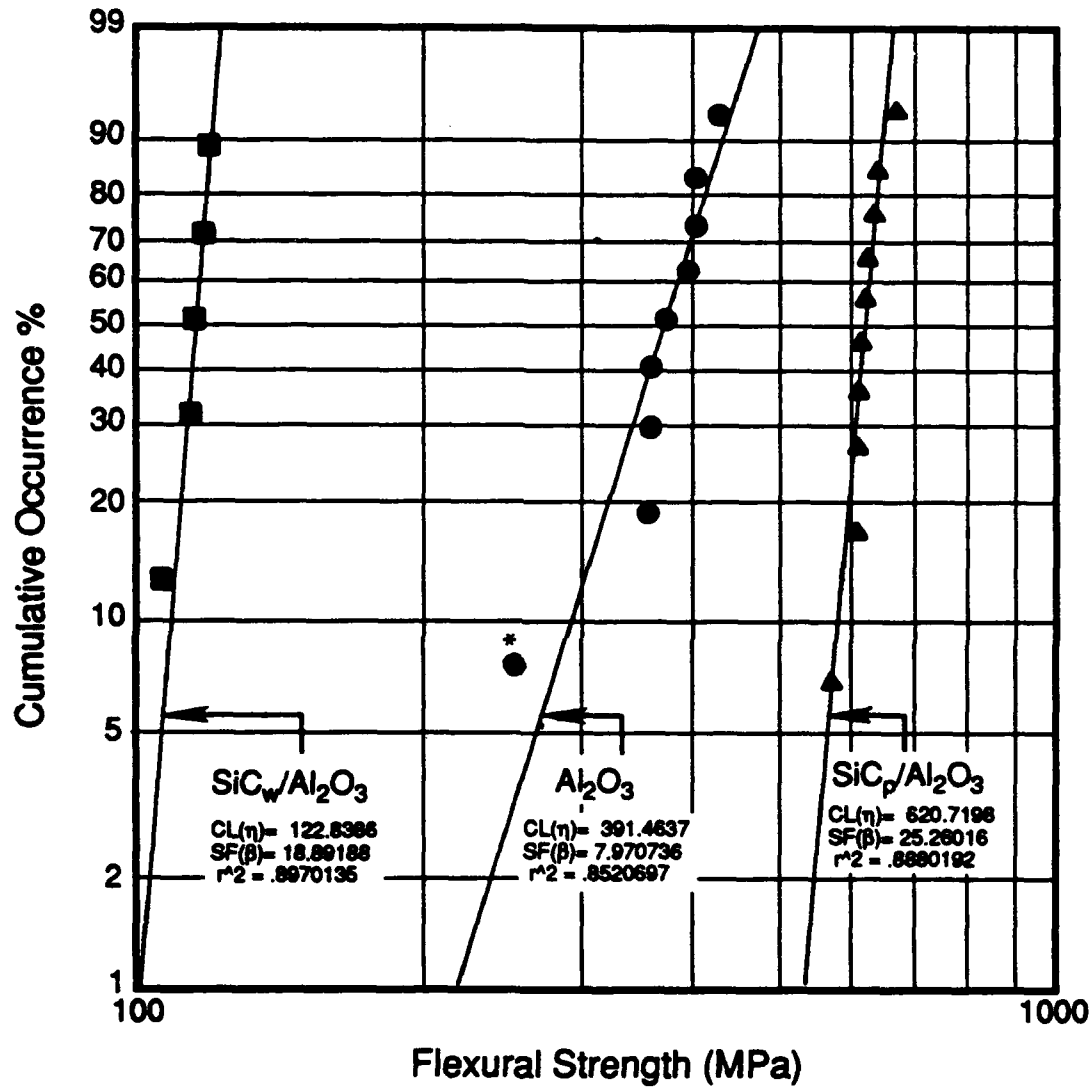
Figure 8 Weibull Plot of Flexural Strength Data

30

Figure 9   Scanning Electron Micrograph of a Fracture Surface of SiC_w/Al_2O_3

Figure 10 Scanning Electron Micrograph of a Fracture Surface of SiC_p/Al_2O_3(Straight Notched Specimen)

32

Figure 11 Scanning Electron Micrograph of a Fracture Surface of SiC_p/Al_2O_3 (Chevron Notched Specimen)
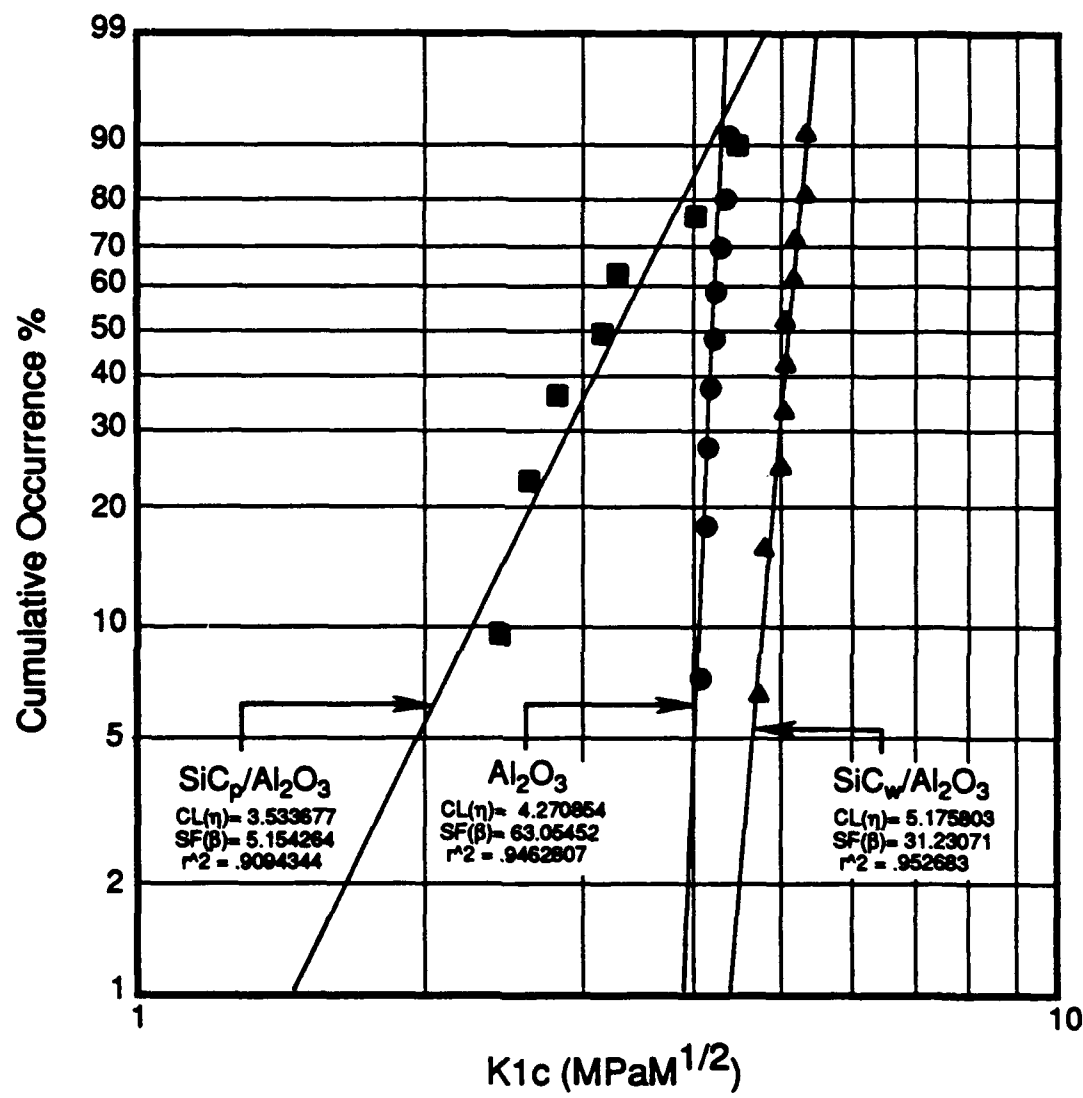
Figure 12 Weibull Plot of Fracture Toughness Data
(Straight Notched Specimen)

34
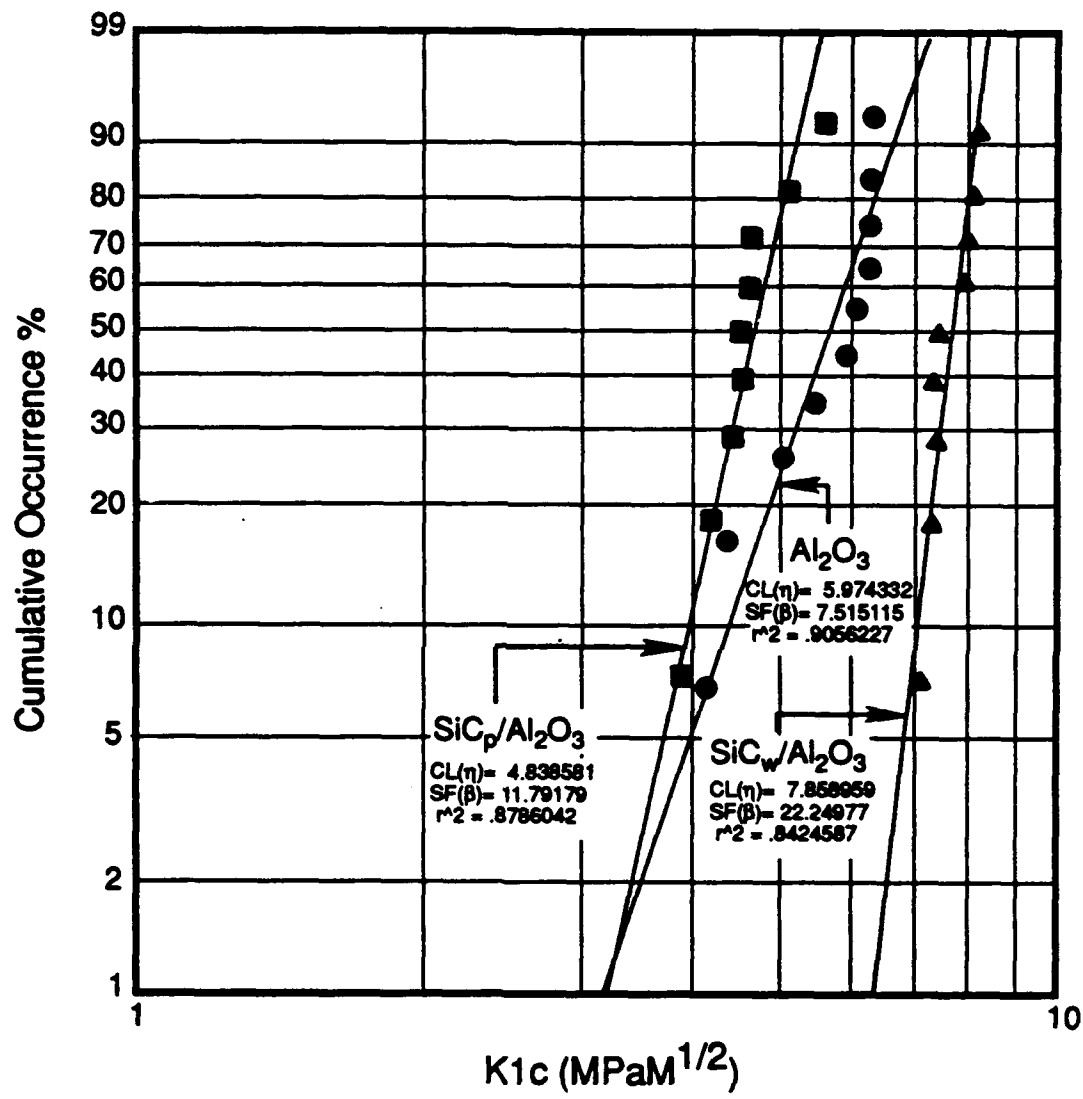
Figure 13 Weibull Plot of Fracture Toughness Data
(Chevron Notched Specimen)

| ALUMINA (EBON-A)	
Manufacturer: Cercom Inc.	
Purity	99.8% pure
Physical Properties:	
Density	3.93 gm/cm³
Flexural Strength	80,000 psi
Compressive Strength	400-500,000 psi
Modulus of Elasticity	57 X 10⁴ psi

Table 1. Manufacturer Data for Aluminum oxide (Ebon A)

SiC Platelets	
Manufacturer: American Matrix Inc.	
Purity	99.99%
Physical Properties:	
Diameter	100-300
Thickness	5-50
Specific Gravity	3.22
Size	100 to 200 mesh

Table 2. Manufacturer Data for Silicon Carbide Platelets

SiC Whiskers: Grade-1	
Manufacturer: Tokai Carbon Co.	
Physical Properties:	
Crystal Type	Beta
Diameter	0.3-0.6
Length	10-15
Aspect Ratio	10-14
Density	3.20 g/cm³
SiC (wt%)	99%
SiO_2 (wt%)	<0.5%
Particulate by wt%	<1%

Table 3. Manufacturer Data for Silicon Carbide Whiskers

FLEXURAL STRENGTH TEST
(BY 4 POINT LOADING)

SAMPLE No.	FLEXURAL STRENGTH MPa		
	Al_2O_3	SiC/Al_2O_3 (Whiskers)	SiC/Al_2O_3 (Platelets)
1	431.18	603.83	120.26
2	356.12	554.04	108.58
3	359.45	593.53	120.51
4	255.87	609.10	123.65
5	403.38	597.42	126.23
6	358.62	629.11	-
7	372.24	622.44	-
8	391.15	665.53	-
9.	403.93	612.16	-
10.	-	598.81	-
Ave.	370.22	608.59	119.85

Table 4   Flexural Strength Data of Al_2O_3 and SiC/Al_2O_3 specimens
(4 point loading)

37

FRACTURE TOUGHNESS TEST
(BY 4 POINT LOADING)

SAMPLE No.	STRAIGHT NOTCH $K_{ic} = MPaM^{1/2}$		
	AL_2O_3	SiC/Al_2O_3 (Whiskers)	SiC/Al_2O_3 (Platelets)
1	4.16	5.09	2.83
2	4.33	5.19	2.45
3	4.17	5.10	3.18
4	4.20	5.29	3.30
5	4.35	4.76	2.64
6	4.26	4.82	4.01
7	4.13	5.35	4.48
8	4.28	5.05	-
9.	4.25	5.18	-
10.	-	5.08	-
Ave.	4.23	5.09	3.27

Table 5   Fracture toughness Data of Al_2O_3 and SiC/Al_2O_3 for Straight
notched specimens (4 point loading)

FRACTURE TOUGHNESS TEST
(BY 4 POINT LOADING)

SAMPLE No.	CHEVRON NOTCH K_{ic} = MPaM$^{1/2}$		
	AL_2O_3	SiC/Al_2O_3 (Whiskers)	SiC/Al_2O_3 (Platelets)
1	5.08	7.14	4.47
2	4.17	7.40	4.25
3	5.49	7.38	4.60
4	6.09	7.37	3.95
5	5.93	8.17	4.58
6	6.30	7.45	5.60
7	6.26	7.99	4.65
8	4.40	8.23	4.65
9.	6.33	8.06	5.11
10.	6.26	-	-
Ave.	5.63	7.69	4.65

Table   6   Fracture toughness Data of Al_2O_3 and SiC/Al_2O_3 for Chevron
notched specimens (4 point loading)

Materials	Flexural Strength 4 Point Bend MPa		Fracture Toughness 4 Point Bend* MPa.M$^{1/2}$		FractureToughness 4 Point Bend** MPa.M$^{1/2}$	
	Weibull Charact- ristic life	Average	Weibull Charact- eristic life	Average	Weibull Charact- eristic life	Average
Al_2O_3	391.46	370.22	4.27	4.23	5.97	5.63
SiC_W/Al_2O_3	620.72	608.59	5.17	5.09	7.86	7.69
SiC_P/Al_2O_3	122.83	119.85	3.53	3.27	4.83	4.65

* Straight Notch
** Chevron Notch

Table 7 Comparison of Weibull Characteristic Life and Average Value of Flexural Strength and Fracture Toughness

Specimen No.	Load(n)	Displacement(mm)		Strain(mm/mm)		Stress(Mpa)	
		Theory	Expt	Theory	Expt	Theory	Expt
1	966.1	0.170554	0.177038	0.001894	0.001942	615.3	596.8
2	886.5	0.156498	0.167107	0.001738	0.001833	564.6	547.4
3	949.6	0.167648	0.174041	0.001861	0.001909	604.8	586.5
4	974.6	0.172045	0.177698	0.001910	0.001949	620.6	601.9
5	955.9	0.116875	0.167335	0.001874	0.001835	608.7	590.4
6	1006.6	0.177699	0.181483	0.001973	0.001990	641.0	621.8
7	995.9	0.175815	0.180264	0.001952	0.001977	634.2	615.1
8	1064.9	0.187986	0.187833	0.002087	0.002060	678.1	657.8
9	979.5	0.172909	0.170485	0.001920	0.001870	623.8	604.9
10	958.1	0.169140	0.165456	0.001878	0.001815	610.2	591.8
Mean	973.8	0.166717	0.174874	0.001909	0.001918	620.1	601.4

Table 8: Comparison of Displacement, Strain and Stress Data for SiC_w/Al_2O_3 Composites

Specimen	Load(n)	Displacement(mm)		Strain(mm/mm)		Stress(Mpa)	
No.		Theory	Expt	Theory	Expt	Theory	Expt
1	689.9	0.145868	0.129108	0.001620	0.001416	439.36	426.03
2	569.8	0.120475	0.116103	0.001338	0.001273	362.88	351.84
3	575.2	0.121604	0.114833	0.001350	0.001259	366.26	355.36
4	409.4	0.086562	0.112827	0.000906	0.001237	260.73	252.83
5	646.3	0.136652	0.119761	0.001517	0.001313	411.60	399.21
6	645.4	0.136465	0.119202	0.001515	0.001307	411.03	398.52
7	573.8	0.121322	0.115087	0.001347	0.001262	365.42	354.39
8	595.6	0.125593	0.112725	0.001398	0.001236	379.31	367.77
9	625.9	0.132325	0.119380	0.001469	0.001309	398.57	386.66
Mean	592.3	0.125207	0.117670	0.001391	0.001290	373.24	365.85

Table 9:   Comparison of Displacement, Strain and Stress Data
for Monolithic Al_2O_3